New, unexpected, and dominant mechanisms in the hydrogen exchange reaction

Stuart J. Greaves,[1,a)] Daniel Murdock,[1,b)] Eckart Wrede,[1,c)] and Stuart C. Althorpe[2]
[1]*Department of Chemistry, University of Durham, South Road, Durham DH1 3LE, United Kingdom*
[2]*Department of Chemistry, University of Cambridge, Lensfield Road, Cambridge CB2 1EW, United Kingdom*

(Received 10 May 2007; accepted 5 March 2008; published online 23 April 2008)

A quasiclassical trajectory study of the state specific $H+D_2(v=0,j=0)\rightarrow HD(v'=0,j'=0)+D$ reaction at a collision energy of 1.85 eV (total energy of 2.04 eV) found that the scattering is governed by two unexpected and dominant new mechanisms, and not by direct recoil as is generally assumed. The new mechanisms involve strong interaction with the sloping potential around the conical intersection, an area of the potential energy surface not previously considered to have much effect upon reactive scattering. Initial investigations indicate that more than 50% of reactive scattering could be the result of these new mechanisms at this collision energy. Features in the corresponding quantum mechanical results can be attributed to these new (classical) reaction mechanisms. © *2008 American Institute of Physics*. [DOI: 10.1063/1.2902972]

I. INTRODUCTION

The hydrogen exchange reaction is the simplest chemical reaction and has, therefore, been extensively studied for over 80 years. A large body of literature including several extensive reviews has been published; see, for example, Refs. 1–8 and references therein.

Advances in the last decade have led to many high quality experiments which report state-to-state differential cross sections (DCSs), which are a stringent test of theory. Experimental agreement with quantum mechanical (QM) calculations is now so good that it is generally accepted that this prototype reaction is fully understood.[8–11] The results from different QM approaches, i.e., different time independent and different time dependent codes, have also converged to agreement.[12,13] While QM can fully reproduce experimental findings, it only has a limited ability to explain the motion of the nuclei during the reactive encounter.

In contrast, the quasiclassical trajectory (QCT) method can explicitly describe the nuclear motion during a reaction. Although QCT cannot accurately reproduce experiments in as much detail as QM, it has been used for a wide number of studies of the hydrogen exchange reaction and has shown surprisingly good agreement with experimental and quantum mechanical cross sections.[14–16] However, QCT can nevertheless give valuable insight into the mechanisms leading to reaction.[17] This has been used to investigate short-lived collision complexes (in terms of time delay)[18,19] and for general investigation of the hydrogen exchange reaction.[20,21] Moreover, we believe that reaction pathways seen in QCT results have a QM equivalent, although features in quasiclassical DCSs may be altered (or even annihilated) by interference effects between different QM reaction pathways.

The dominant mechanism in the hydrogen exchange reaction is accepted to be direct recoil,[1,22] which leads mainly to backward scattering. The direct recoil mechanism is a consequence of the linear minimum energy path (MEP) and transition state of the H_3 potential energy surface (PES). At low collision energies, reactions can only proceed via almost linear geometries (close to the MEP) leading to collinear, end-on collisions of the reagents. In this collinear picture, the vibrational excitation of the product molecule is determined by the closest approach of the atoms, which will form the product molecule during the reactive encounter. At low energies, the closest approach corresponds to the inner turning point of a low vibrational state. At increasing collision energy, this picture would inevitably lead to higher vibrational excitation because of the much closer approach of the incoming atom: In contrast, trajectories with low rotational excitation, which should correspond to collinear approaches, are predominantly formed in low vibrational states. Therefore, mechanisms other than the direct recoil must be at work. At higher collision energies, the reaction path can significantly deviate from the MEP; thus, the reaction is no longer restricted to a direct recoil mechanism. Indeed, at collision energies between 1.6 and 1.9 eV, a different reaction mechanism was required to explain forward-scattered $HD(v'=3,j'=0)$ products.[23–25] We have examined the short-lived collision complex invoked to explain this forward scattering in an adjacent paper.[26]

Standard plots of PESs highlight the MEP as they use internal coordinates, e.g., two distances at fixed bending angle (linear) showing the reactant and product channels. We find it more instructive to plot the H_3 potential at fixed diatom distance as a function of position of the third atom (see Fig. 1). This shows the steep repulsive walls around the diatom, the linear well (which corresponds to the saddle point on the MEP) and a further striking feature; the H_3 PES has a

[a)]Present address: School of Chemistry, University of Bristol, Bristol BS8 1TS, U.K.
[b)]Present address: Department of Chemistry, Yale University, P.O. Box 208107, New Haven, Connecticut 06520-8107.
[c)]Author to whom correspondence should be addressed. Electronic mail: eckart.wrede@durham.ac.uk.

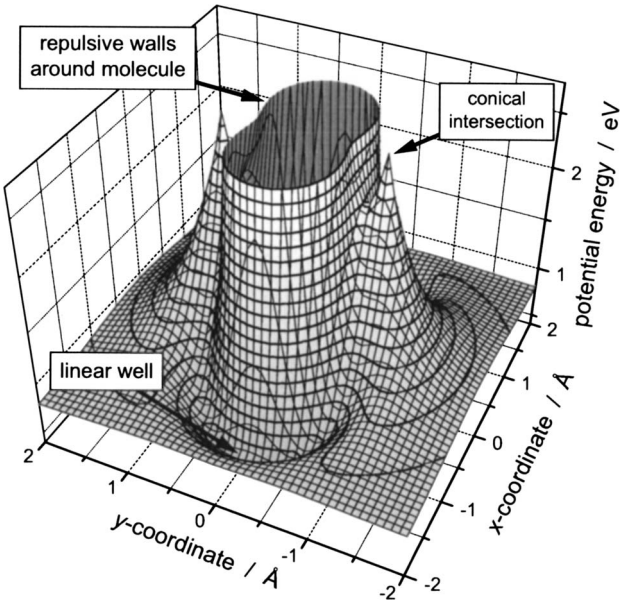

FIG. 1. Surface plot of the H_3 PES in Cartesian coordinates. The potential is plotted as a function of the position (x,y) of the third H atom with respect to the center of mass of the H_2 diatom. The H_2 lies on the x axis and the potential is shown at the fixed diatomic distance $r=1.044$ Å. The conical intersection (CI) to the first excited state which appears at equilateral triangular geometry is indicated. Note that the three-dimensional potential is cylindrically symmetric around the x axis.

well characterized conical intersection (CI) at equilateral triangular geometries. At small internuclear *BC* separation the CI moves into the region of high repulsive potential surrounding the *BC* diatom and is, therefore, less prominent. At large *BC* separations, the CI becomes a more prominent topological feature on the PES, as it is no longer in the region of high potential surrounding the *BC*.

The influence of this CI on the nuclear dynamics has so far been mainly associated with the geometric-phase (GP) effect.[17,27] We do not consider this very special quantum effect in this paper but examine the broader influence of the repulsive slope around the CI on the dynamics of this reaction.

In Sec. II, we present the particulars of the QCT methodology. Section III describes our QCT calculations and results, Sec. IV covers our analysis of the new mechanisms, and our conclusions are presented in Sec. V.

II. METHODOLOGY

The QCT methodology was adapted from Refs. 20 and 28. By following the standard procedure, the reactant D_2 molecule is prepared in a discrete internal energy state corresponding to the initial (v,j) quantum state. Having selected the rovibrational state and the fixed collision energy (E_{col}), the other initial collision variables are randomly selected from the relevant classical distributions. The fixed stepsize Hamming predictor-corrector method[29] was used to integrate the equations of motion. The conservation of both the total energy and the total angular momentum was monitored to ensure the accuracy of the integration. The (v',j') quantum numbers of the outgoing molecule were assigned for a given rotational angular momentum by equating the internal energy

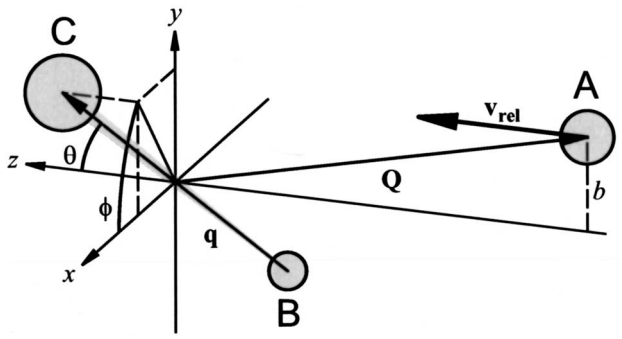

FIG. 2. The collision parameters (see text) and Jacobi coordinates $(\mathbf{q},\mathbf{Q})$ used to define the initial geometry of an $A+BC$ system for QCT calculations.

to the full Dunham expansion of the rovibrational energies of the HD molecule.[30] The QCT method is well described in detail in Ref. 28 and, thus, we will only highlight the aspects pertinent to this work.

A. Initial conditions

The outcome of each trajectory is determined by its initial parameters which define the initial geometry and dynamic state of the system and make each trajectory unique. Besides the rovibrational state and the collision energy, there are five collision parameters, some of which are shown in Fig. 2.

We define the center of mass of the *BC* reactant molecule (D_2) to be at the origin and the H atom to start in the yz plane, with the initial relative velocity vector $\mathbf{v}_{rel}$ directed along the positive z axis. The collision parameters are (i) the impact parameter b, corresponding to the initial y coordinate of the reactant atom A (H atom), (ii) the polar orientation angle θ of the *BC* internuclear axis ($\mathbf{q}$ vector in Fig. 2), i.e., the angle between $\mathbf{q}$ and the positive z axis, (iii) the azimuthal orientation angle ϕ of the *BC* axis, defined as the angle between the projection of $\mathbf{q}$ on the xy plane and the positive x axis, (iv) the orientation of *BC* angular momentum relative to a reference vector normal to the *BC* internuclear axis (this is not used in the present work as D_2 has no initial rotational angular momentum, $j=0$), and (v) the phase of the *BC* vibration.

B. First impacts

A useful tool to characterize and understand the different reaction mechanisms is to identify the geometry of the collision complex at the first impact of the incoming atom (H atom) on the repulsive part of the H_3 potential surrounding the reactant molecule (D_2). An impact can be defined as a maximum in the potential energy and, thus, a minimum in the kinetic energy of the HD_2 system. However, the total potential energy V_{tot} changes with the vibrational motion of the reactant molecule before the HD_2 complex is formed, and likewise, with the product vibration. We, therefore, define an adjusted potential, $V_{adj}=V_{tot}-V_{mol}$, where V_{mol} is the potential energy of the diatomic defined as the pair of atoms with the current shortest internuclear distance. Figure 3 shows the time dependence of the total and adjusted poten-

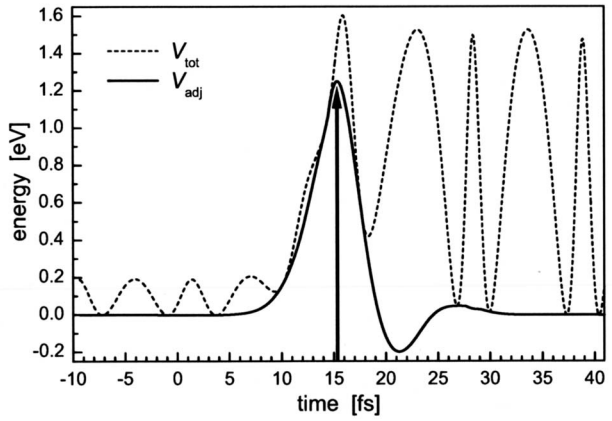

FIG. 3. Total potential energy (V_{tot}) and adjusted potential ($V_{adj}=V_{tot}-V_{mol}$) as a function of time for a trajectory leading to a HD($v'=3,j'=2$) product. The impact of the incoming atom on the repulsive potential of the D_2 reactant molecule is defined as the first maximum in V_{adj}, which is highlighted by the arrow, see text.

tials of a trajectory leading to a HD($v'=3,j'=2$) product as an example. An impact is defined as the first maximum in V_{adj}, as indicated by the arrow in Fig. 3.

The relative positions of the three atoms were recorded at the first impact. This allowed the paths of the atoms to be overlaid on a Cartesian contour plot of the PES at the point of impact which we call "impact diagrams," see later. These impact diagrams were used to clarify the workings of the mechanisms.

C. Near-side/far-side scattering

An advantage of the QCT method is the ability to distinguish between products scattered into the positive y hemisphere, i.e., the same side as the impact parameter b (see Fig. 2), and those scattered into the negative y hemisphere, called *near-side* and *far-side* scattering, respectively.[31] By testing the y component of the final relative velocity vector ($\mathbf{v}'_{rel}$) of the departing D–HD products, we identify scattering into the near side (positive y component) and far side (negative y component). To distinguish between near- and far-side scattering, we define the deflection angle Θ as the positive scattering angle, $\Theta=+\theta_{scatt}$, for near-side scattering and as the negative scattering angle, $\Theta=-\theta_{scatt}$, for far-side scattering.

III. CALCULATIONS AND RESULTS

Five million trajectories for the H+D$_2$($v=0,j=0$) $\rightarrow$HD+D reaction were propagated on the BKMP2 PES (Ref. 32) at a collision energy $E_{col}=1.85$ eV. The initial and final atom-diatom distance was 6 Å and the maximum impact parameter was 1.35 Å. The fixed integration stepsize was 3.5×10^{-17} s to ensure the conservation of the total energy and angular momentum to be better than 5 and 10 ppm, respectively. 1 082 947 trajectories were found to be reactive with 2337 in the HD($v'=0,j'=0$) product state.

The QCT method generates continuous product state quantum numbers which are usually rounded to the nearest integer (histogram binning method); i.e., $v'_{QCT}=0.5-1.5$ is assigned to $v'=0$. Consequently, each quasiclassically assigned quantum state has a range of internal energies and, therefore, a corresponding spread of product velocities. To clarify the time dependent evolution of trajectories and the following identification of novel reaction mechanisms, only trajectories with a vibrational quasiclassical quantum number in the range of $v'_{QCT}=0.9-1.1$ were analyzed. As only 470 trajectories were found in this restricted HD($v'=0,j'=0$) quantum state, we also include the 1760 trajectories with $j'=1$ in our analysis.

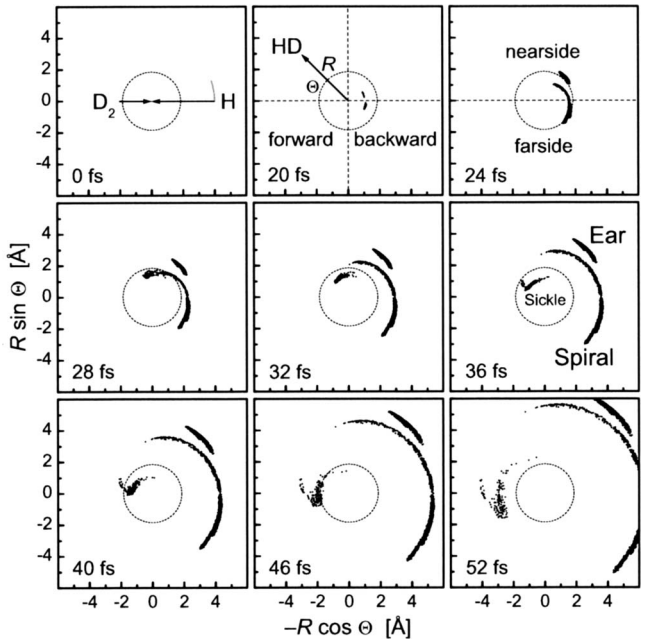

FIG. 4. Snapshots representing the product densities for H+D$_2$($v'=0,j'=0$)$\rightarrow$HD($v'=0,j'=0-1$)+D at $E_{col}=1.85$ eV in three dimensions. Frame 0 fs shows the relative velocities of the reagents in the center-of-mass frame. Each point represents the position of a HD product for a single trajectory, as defined by its deflection angle Θ and distance from the the center of mass, see frame 20 fs. The central circle gives an indication of the size of the interaction region, and the arrow in frame 20 fs is pointing in the forward-scattered direction. The near-side and far-side scattering regions are delineated in frame 24 fs. The three clear regions of the scattered products, ear, spiral, and sickle are labeled in frame 36 fs.

A. Time-space evolution of products

Recent wavepacket calculations for this system have demonstrated that different reaction mechanisms can be elucidated by monitoring the time evolution of the product flux as a function of scattering angle.[23,24] We adapt the quantum approach to produce equivalent temporal snapshots of the HD products. A trajectory was deemed to have progressed to a state where the HD product molecule is formed after the first minimum in the H–D internuclear distance (inner turning point of HD product vibration). The position of the HD product center-of-mass is then plotted as a function of the D–HD distance R and deflection angle Θ relative to the initial direction of the H atom (i.e., in planar polar coordinates $R\cos\Theta$ versus $R\cos\Theta$.

Figure 4 shows temporal snapshots of the densities of HD($v'=0,j'=0-1$) products as a scatter plot. Note that due to the restriction in v', all products have almost the same speed. Thus, the distance from the center is a measure of the

time delay of the trajectory, i.e., the time spent in the transition state region. The further products are plotted from the center the earlier they are formed. Three different scattering regions can clearly be identified in Fig. 4 (labeled in frame 36 fs).

The products with the longest time delay are scattered into the forward region and are labeled "sickle." The "spiral" covers the largest range of deflection angles, from early formed backwards scattered products on the far side ($\Theta \approx -130°$) to later formed sideways scattered products ($\Theta \approx +70°$) on the near side. The correlation between the deflection angle and the time delay gives the spiral its distinctive shape. If higher rotational levels of the HD products are included ($j'=0-3$), then a continuation of the spiral is observed, filling the gap between sideways scattering and the fraction of the spiral which is forward scattered. The latter fraction can be most clearly seen in frame 46 fs of Fig. 4 adjacent to the sickle at $\Theta \approx 0°$. For reasons which will become apparent later, the spiral has been subdivided into its near-side and far-side scattered regions. The third and most distinct region, labelled "ear," consists of early formed products which scatter into a narrow range of near-side deflection angles: $\Theta = 110° - 150°$. Three similar regions have been noted before in a symmetrized (i.e., non-near/far-side resolved) scattering angle versus trajectory time correlation plot for $H+D_2$ collisions at $E_{col}=1.0$ eV but were never separately examined.[18]

The three, clearly distinct regions would seem to indicate that three separate reaction mechanisms are at work here. Note that the ear and the far-side part of the spiral consist of trajectories with the smallest time delays typical for fast and direct reaction mechanisms. The forward-scattered sickle features the longest time delays indicating an indirect mechanism, whereas the increasing time delay from backward to forward scattering of the spiral hints at a gradually changing mechanism.

IV. ANALYSIS AND DISCUSSION

In this section, the correlations between initial conditions and product properties will be investigated along with an analysis of how the hydrogen atom "impacts" upon the repulsive potential around the D_2 molecule. Mechanisms can be confirmed by analyzing the configuration of the atoms at the point of impact and the angle of the impact from the path of the incoming H atom, which heavily relies on the initial orientation of the system.

A. Correlations of initial conditions

We consider two-dimensional collisions restricted to the *yz* plane first. Figure 5 shows the correlation between the impact parameter b and initial polar orientation angle θ (cf. Fig. 2). The separate regions of the snapshot diagram were found to have highly correlated and distinct initial conditions. This indicates that the scattering regions have different mechanisms which derive from the initial alignment of the atoms.

While the two-dimensional case is very instructive to identify the correlations, it is imperative to generalize this

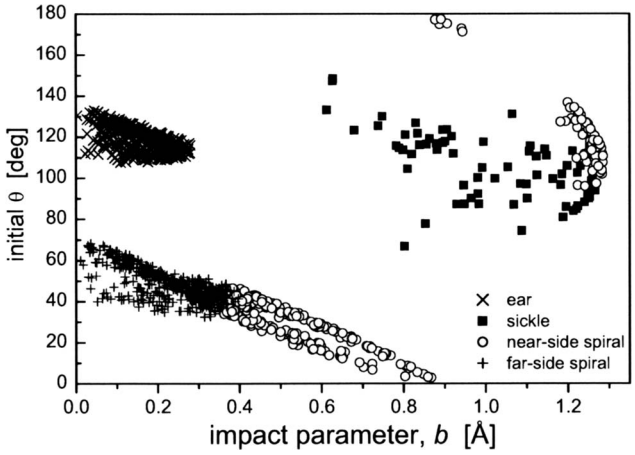

FIG. 5. Correlation between impact parameter b and initial polar orientation angle θ for trajectories leading to HD($v'=0, j'=0-1$) products in the three regions, ear (×), spiral (○, +), and sickle (■). The trajectories were restricted to two dimensions, in the *yz* plane, at a collision energy of 1.85 eV.

picture for the full three-dimensional case. Figure 6 combines the correlations between the initial geometry, i.e., the orientation of the D_2 axis and the impact parameter, and the HD product's deflection angle. The orientation of the D_2 molecular axis is now plotted as the projection of the leading D atom onto the *xy* plane, as depicted in panel (a) of Fig. 6. To eliminate the effect of the vibrational motion, we plot this projection for the fixed D_2 equilibrium bond length. Initial D_2 orientations perpendicular to the direction of the incoming H atom would lie on the circle in panel (b) and orientations along the *z* axis at the origin. Panel (c) shows the correlation between the *y* coordinate of the projection and the impact parameter which is equivalent to Fig. 5 for the two-dimensional case but now includes out-of-plane initial orientations. A collinear trajectory would be represented by a point at the origin in panel (b) and a point at zero impact parameter in panel (c). Finally, the correlation between the impact parameter and the deflection angle is shown in panel (d).

Figure 6 again highlights the clear correlations between the initial conditions and the deflection angle for the different scattering regions. Trajectories in the ear and far-side spiral regions are characterized by D_2 orientations nearly perpendicular to the relative velocity (*z* axis) and low impact parameters ($b<0.3$ Å). Furthermore, both regions show scattering into very limited regions of space but with opposing deflection angles into the near side (ear) and the far side (spiral). Note that both sets of trajectories would lead to similar scattering angles as an experiment cannot distinguish between near- and far-side scattering due to the cylindrical symmetry of the collisions around the relative velocity.

The most notable feature of the near-side spiral is that its initial geometries are very planar. The *y* projection of the initial D_2 orientation shows an almost linear relationship with the impact parameter [Fig. 6(c)], which, in turn, exhibits a near linear relationship with the deflection angle [Fig. 6(d)]. Note the isolated fraction of trajectories at high impact parameters which scatter into the forward direction and which are hidden among the points of the ear at the top of panel (b). As commented on earlier, if trajectories with

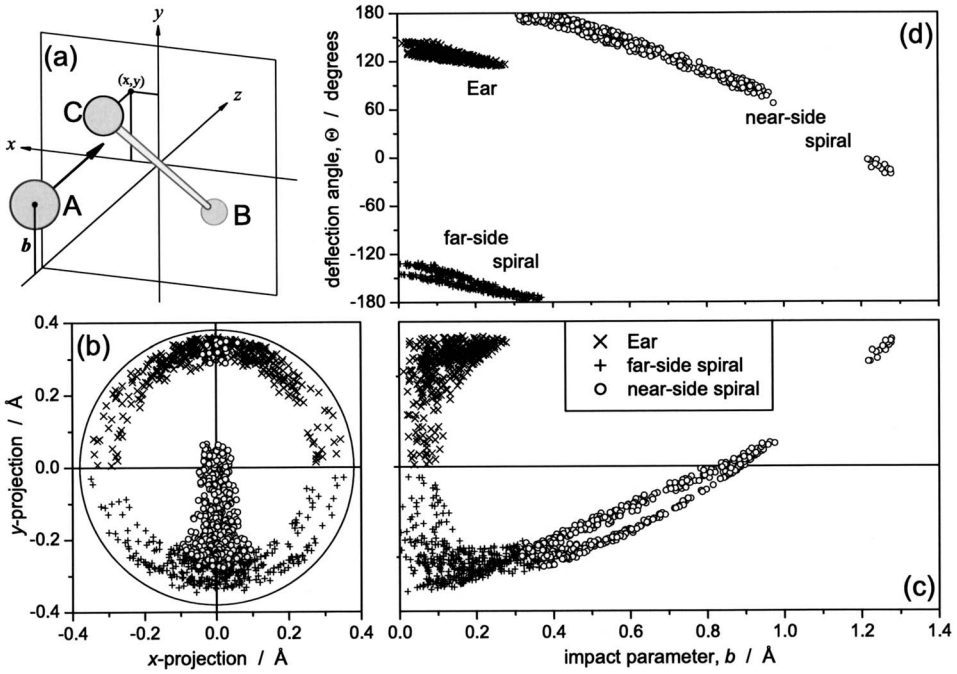

FIG. 6. Plots showing the correlation between impact parameter b, D_2 axis orientation, and deflection angle Θ for ear ($\times$), near- ($+$), and far-side ($\bigcirc$) spiral trajectories in the HD($v'=0, j'=0-1$) state at $E_{col}=1.85$ eV. (a) Initial conditions for a trajectory: Impact parameter b and location of the leading D atom projected onto the xy plane, shown in panel (b). The circle in panel (b) represents the outermost position possible for a leading D atom (i.e., for a perpendicular D_2 axis orientation). (c) Correlation between impact parameter and the initial y coordinate of the leading D atom. (d) Correlation between impact parameter and scattering angle. The far-side spiral is shown to be the continuation of the LID mechanism, with all trajectories having a side-on approach to the D_2. The near-side spiral is shown to be highly planar in nature, with a strong correlation between impact parameter and deflection angle.

higher product rotational states are included ($j'=0-3$), the main and isolated parts of the near-side spiral are continuously joined. The sickle region exhibits a less clear picture and because of its small statistical weight is not included in Fig. 6.

In the hard-sphere scattering model, the outcome of every collision is determined by the location of the impact of the two spheres. In a similar fashion, the initial geometries of the H+D_2 collisions discussed here will govern where the incoming H atoms will impact on the D_2 molecules and, thus, will determine the outcomes of the trajectories.

B. Early formed trajectories

The ear region contains trajectories that form earliest and which scatter into a well-defined and restricted angular range (see Fig. 4). It is produced by a separate unique mechanism due to the initial orientation of the system, as demonstrated by Figs. 5 and 6. This initial orientation causes the H atom in the ear trajectories to approach the D_2 side on with a low impact parameter and, therefore, to "impact" on the H_3 PES on the sloping potential that surrounds the CI; this can be seen in the impact diagrams in Fig. 7. The H atom impacts on the sloping potential on the same side as the foremost D atom, which causes the H atom to be deflected upwards, onto this foremost D atom, as shown in panels (a)–(c) in Fig. 7.

The far-side spiral feature also contains some of the earliest formed trajectories, on a similar time frame to the ear, i.e., with little time delay. The impact diagrams (d) and (e) in Fig. 7 show the similarity of the far-side spiral trajectories to the ear trajectories. It is clearly seen that the far-side spiral is the continuation of the same mechanism, in which the perpendicular alignment of the D_2 [see Fig. 6, panel (b)] causes the sloping potential around the CI to deflect the hydrogen downwards toward the foremost deuterium in the lower hemisphere.

C. Low impact deflection mechanism

The mechanism which leads to the ear and far-side spiral scattering regions requires low impact parameter H atoms which impact upon the sloping potential surrounding the CI on the same side as the foremost D atom. The sloping potential then deflects the H atom toward this foremost deuterium. As such, we have named it the low impact deflection (LID) mechanism. Because of the low impact parameters, very little rotation is imparted onto the D_2 at collision. As the interaction with the sloping potential around the CI is brief, the mechanism is very direct, showing no signs of complex transition state behavior.

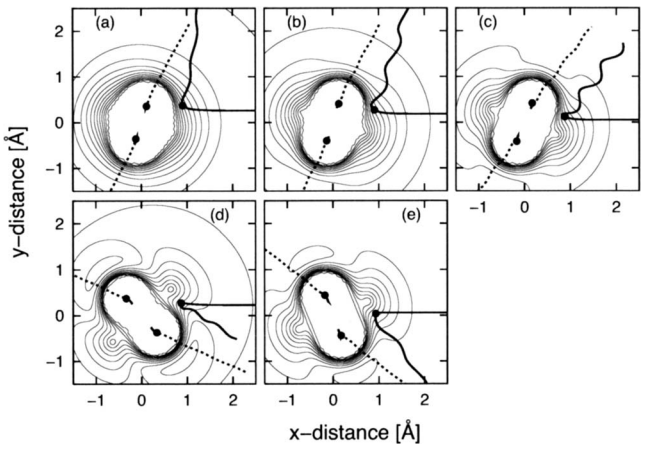

FIG. 7. Impact diagrams, see text for details. Panels (a)–(c) show impact diagrams for trajectories from the ear region. The trajectories with the highest impact parameter are the most sideways scattered. Panels (d) and (e) show impact diagrams for the far-side spiral region. The trajectories with the lowest impact parameter are the most sideways scattered. The dotted lines represent the motion of the D atoms; the H atom (thick solid line) approaches from the right at an impact parameter b above $y=0$; its impact is marked with a ●. The contours represent the H_3 PES at the impact geometry. The trajectories were restricted to two dimensions, in the yz plane, at a collision energy of 1.85 eV.

Figure 7 demonstrates the impact parameter dependence of the LID mechanism: As the impact parameter decreases [from panels (a) to (c)], the scattering angle becomes larger. The deviation in the path of the H atom caused by the sloping potential around the CI is obviously dependent on the prominence of the CI and, hence, on the value of the D_2 separation q at the point of impact. The shape of the potential in this location causes the ear trajectories to be scattered sideways. This mechanism cannot produce backward scattering ($\Theta = 180°$) as the D_2 axis would have to be perpendicular to an incoming hydrogen with zero impact parameter. Such a trajectory would be nonreactive as the CI would deflect the hydrogen away from the deuterium molecule.

The side-on nature of the trajectories is in stark contrast to the case of the recoil mechanism that is assumed to be prevalent for this reaction.[1,22] The correlation and impact diagrams, Figs. 6 and 7, respectively, clearly highlight the different orientations and geometries upon impact between the direct recoil case, which is dominated by collinear collisions, and the LID case with its side-on collisions. The deflection of the H atom by the CI's sloping potential in the LID mechanism allows the trajectory to excite the $v' = 0$ state through a softer impact on the D atom. The HD product is set up in a geometry which corresponds to the inner turning point of the $v' = 0$ vibration. This is in contrast to the hard impacts seen in collinear trajectories at this collision energy which inevitably set up the HD products at the inner turning points of highly excited vibrational states. The collinear nature of these hard impacts is described by the direct recoil mechanism, which is seen in the trajectories leading to HD($v' = 3, j' = 0$) products, as will be discussed in our adjacent paper.[26]

D. Near-side spiral

The near-side spiral trajectories cover the full ranges of both the scattering angle and trajectory time, from the early product forming backward scattering trajectories through to the late forming forward scattering trajectories.

Again, the highly correlated initial conditions for these trajectories demonstrate (see Figs. 5 and 6) that a specific orientation of the system is required for spiral trajectories, which also shows a strong correlation with the deflection angle. The spiral trajectories are very planar, as demonstrated by the clustering of the trajectories around the yz plane in panel (b) of Fig. 6; thus, the D_2 axis orientation is controlled by the initial polar orientation angle θ. As the impact parameter increases and θ decreases, the deflection angle decreases, becoming more forward in character. The system becomes less planar in the lower half of panel (b) of Fig. 6 as it overlaps with the D_2 axis orientation seen for the far-side spiral. The overlap at the top of panel (b) is not due to a similar effect, as the ear trajectories at that point have low impact parameters and the spiral trajectories have large impact parameters [as shown in panel (c)] and, consequently, do not impact at the same point on the PES.

Near-side spiral impact diagrams are shown for a range of deflection angles in Fig. 8. Just as for the LID mechanism, all trajectories show interaction with the sloping potential around the CI. These diagrams also contain information about the rotation of the system; the sharp bends in the motion of the D atoms (dotted lines) indicate the magnitude of the rotation.

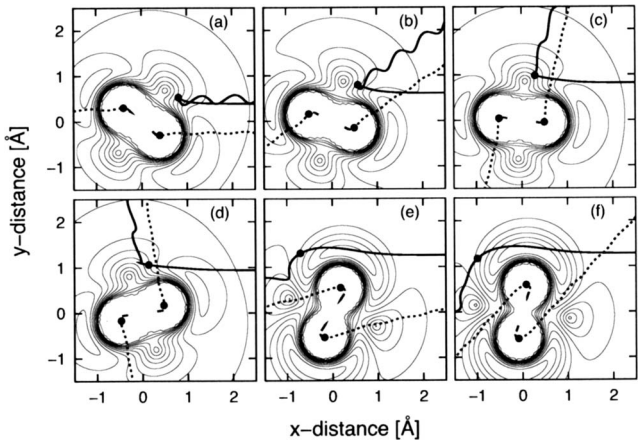

FIG. 8. Impact diagrams (see Fig. 7) for the near-side spiral region. Deflection angles for the trajectories shown in panels (a)–(f) are, respectively, 179°, 146°, 104°, 81°, −11°, and −46°.

The most forward scattered trajectories display H atom impacts on the CI's sloping potential on the "far side" of the D_2, relative to the H atom approach, after they passed the leading D atom at large impact parameter, as shown in panels (e) and (f). The impacts for the near-side spiral occur at larger D_2 separations than for ear trajectories (cf. Fig. 7) when the CI is more prominent.

E. Revolving door mechanism

Scattering into the near-side spiral region is controlled by what we have named the revolving door mechanism. This mechanism is clearly demonstrated in the movie sequence (Fig. 9) and the following description:[33] Frame 0–15 fs, the hydrogen (●) approaches the D_2 molecule at large impact parameter. Frame 15–18 fs, the D_2 bond stretches as the H atom flies past the end of the D_2. Frame 18–22 fs, the H atom is slowed by the increasing potential gradient around the CI. Frame 22–25 fs, the H atom has transferred most of its translational energy to the D_2 via the "lever arm" of the CI causing the D_2 to rotate about its center of mass. Frame 25–29 fs, the continued rotation moves the linear well toward the almost stationary H atom, which starts to "fall" into it. Frame 29–32 fs, this causes the D_2 bond to stretch even further, deepening the potential well. Frame 32–36 fs, the H atom impacts on the D atom at the inner turning point of the $v' = 0$ vibration to set up the product state. Frame 36–39 fs, the H atom is now trapped in the increasingly deep well as the D_2 bond breaks. Frame 39–55 fs, the HD and D products are formed and scatter.

The sloping potential around the CI acts as a lever to rotate the D_2 bond, and in transferring its kinetic energy to the D_2 rotation, the H atom is stopped and, therefore, able to impact with the D atom when the D_2 rotation catches up with it.

The revolving door mechanism was so named because of the similarity it shows to the probable outcome of running

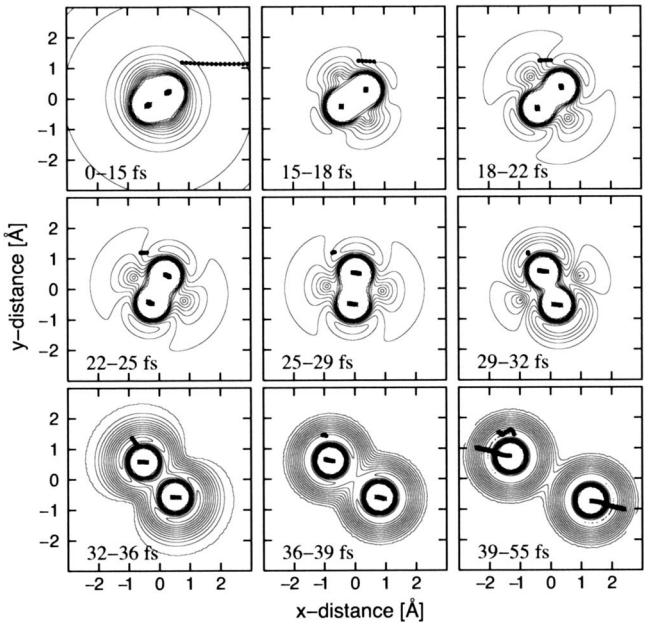

FIG. 9. Reaction mechanism diagram for a typical trajectory in the near-side spiral region of HD($v'=0, j'=0-1$) product state. The H atom position during each frame is represented by ●, and the D atoms by ■, the contours represent the H_3 PES at the middle time step of each frame. See text for details. The trajectory was restricted to two dimensions, in the *yz* plane, at an energy of 1.85 eV.

into a revolving door; i.e., you stop on hitting one of the doors but cause the door to rotate, then another of the doors hits you in the back and pushes you forwards.

For the HD product to be scattered forwards, the D_2 has to rotate through a large angle and, therefore, requires a large impact parameter to allow maximum torque at impact. On going from forward to backward scattering, the amount of D_2 rotation required is diminished. As the impact parameter increases [panels (a)–(f) of Fig. 8], the deflection angle concertedly decreases. These factors lead to a decrease in the torque exerted on the D_2 and, therefore, less rotation.

The longer time delays of the forward-scattered trajectories are due to the greater distances traveled by the hydrogen before the first impact and the time required for the D_2 rotation. Backward scattered trajectories have earlier impacts and require less rotation and, consequently, take less time. The trajectories that are scattered sideways with similar scattering angles to the ear take longer times than the ear trajectories because of the extra time required for the impact, energy transfer, and rotation.

Because of the nature of the rotation required for the revolving door mechanism, it has to operate in a planar system. If the system was not planar, then the D_2 rotation, caused by the impact of the H atom on the CI, would lead to higher rotational excitation of the products.

The collision with the sloping potential surrounding the CI slows the motion of the hydrogen, allowing it to match speeds with, and impact upon, the deuterium at the inner turning point of the $v'=0$ vibration, allowing excitation into this product state. This leads to the conclusion that the revolving door mechanism, similar to the LID mechanism, is a way of allowing access to lower vibrational states by temporarily converting excess collision energy into D_2 rotational energy before being converted back again into translational energy upon release of products.

F. Sickle

The sickle trajectories scatter in the forward direction and have the longest total times of the three regions in the snapshots, but the trajectory time shows little dependence on deflection angle in contrast to the spiral. The initial conditions are also less correlated than for the ear or spiral, with no discernible dependences, apart from requiring a relatively large impact parameter and near perpendicular D_2 axis orientation (see Fig. 5).

It is important to note that none of the impacts show any interaction with the CI; therefore, the excess energy is converted via other mechanisms. Sickle trajectories display a short term reactive intermediate, which undergoes symmetric stretching motions. Similar trajectories were found in the HD($v'=3, j'$) products of the title reaction and will be discussed in an adjacent paper.[26] These trajectories correspond to the well-known forward-scattered time-delayed mechanism, which was first conclusively identified by a combination of quantum wavepacket calculations and experimental measurements.[23] Later work[25] showed that the mechanism was caused by a superposition of "quantum bottleneck states," which cause the system to linger for about 10–25 fs on top of the effective adiabatic-reaction barriers. Interestingly, earlier QCT calculations were able to capture about one third of this highly QM mechanism,[7,15,18] which is consistent with the appearance of the sickle in Fig. 4. Further analysis of the sickle was prevented by the small number of trajectories in the region.

G. Comparison with HD($v'=0, j'=0$) QM snapshots

QM snapshots for HD($v'=0, j'=0$) products, adapted from Ref. 34, are shown in comparison with the QCT snapshots (Fig. 4) in Fig. 10. Note that these wavepacket calculations cover a wide range of collision energies, 1.1–2.25 eV, and so give a range of product scattering velocities. In contrast, the QCT snapshots (Fig. 4) represent trajectories which have a single collision energy of 1.85 eV. Hence, a detailed, quantitative comparison between the QCT and quantum results would require many more trajectories to be propagated to capture the spread of energies in the wavepacket.

However, a crude comparison between the QCT and quantum results is all that is required to establish, almost beyond a doubt, that the new LID and revolving door mechanisms are present in the quantum results. Figure 10 overlays the QCT and quantum snapshots at 32 and 46 fs. It is clear that the two "wings" which appear in the quantum probability near deflection angles $\Theta = \pm 135°$ in frame 32 fs of Fig. 10 are almost certainly produced by the LID and revolving door mechanisms. The inner part of the backward-scattered probabilities corresponds to the direct recoil product (which is concentrated in the lower energy part of the packet). The pronounced gaps between these various components of the

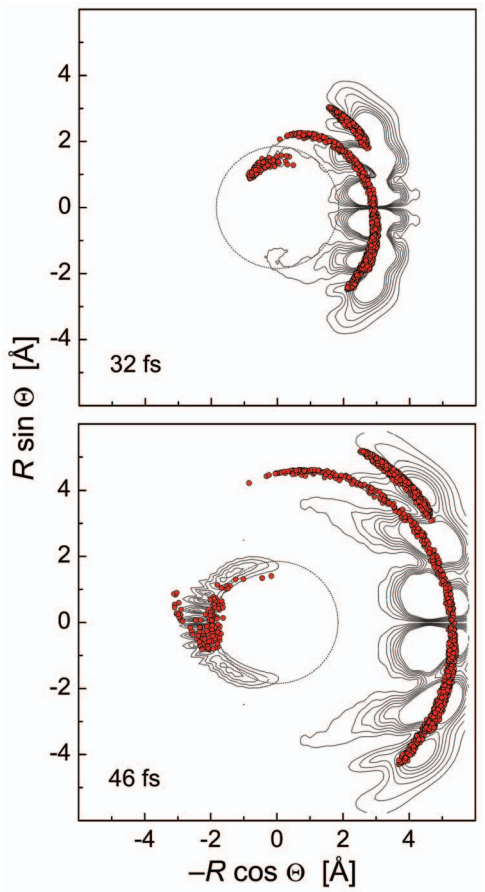

FIG. 10. (Color) Comparison of QM and QCT snapshots for the $H+D_2(v'=0,j'=0) \rightarrow HD(v'=0,j'=0)+D$ reaction. Snapshots from the quantum wavepacket simulation result from a range of collision energies, $E_{col}=1.1-2.25$ eV, adapted from Ref. 34. The contours are obtained from the complete wavefunction of the reaction and show the time evolution of the $HD(v'=0,j'=0)$ product, as a function of the deflection angle Θ. The QCT snapshots are taken from Fig. 4. The dashed circles are of radius $R=1.85$ Å and give a rough indication of the extent of the transition state region.

backward-scattered probability are almost certainly caused by quantum interference between the direct recoil, LID, and revolving door mechanisms.

The forward-scattered part of the quantum probabilities almost directly line up (in frame 46 fs of Fig. 10) with the QCT sickle. As mentioned above, this is what would be expected, since the sickle is produced by the time-delayed, forward-scattered mechanism.[23] The rapid oscillations seen in the forward-scattered wavepacket are not present in the QCT sickle, since they are produced by quantum interference between the near-side and far-side pieces of the packet. This effect is also called Glory scattering, see Refs. 35 and 36.

H. Significance of new mechanisms

The reactive cross section for a batch of trajectories is given by[28]

$$\sigma = \pi b_{\max}^2 \frac{n}{N}, \tag{1}$$

where $b_{\max}$ is the maximum impact parameter sampled (1.35 Å), n is the number of trajectories with a given property (e.g., scattered into a given $HD(v',j')$ quantum state or having a particular mechanism), and N is the total number of trajectories run.

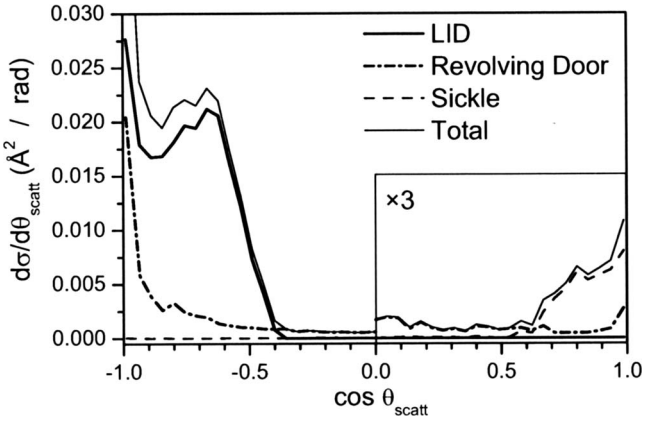

FIG. 11. Cross section of the new mechanisms in the $H+D_2(v'=0,j'=0) \rightarrow HD(v'=0,j'=0-1)+D$ reaction at a collision energy of 1.85 eV as a function of scattering angle, showing the dominance of the LID mechanism.

To illustrate the relative significance of the new mechanisms described above, a histogram binned in the cosine of the scattering angle and Eq. (1) was used to produce a DCS. The cross sections of each mechanism are compared to the total DCS for the $HD(v'=0,j'=0-1)$ product states in Fig. 11. The results for 5×10^6 three-dimensional trajectories (without quasi-v' restriction) carried out at an E_{col} of 1.85 eV were used for the calculation of the DCS.

The DCS clearly shows that the majority (74%) of scattered $HD(v'=0,j'=0-1)$ flux arises from the direct LID mechanism. The revolving door corresponds to 21% of the total $HD(v'=0,j'=0-1)$ scattering and is, therefore, statistically significant. The sickle trajectories only correspond to 5% of the classical scattering but may be more significant in the QM picture.

I. Influence of the conical intersection

To assess the significance of the new mechanisms to the total reactive scattering, a series of geometric, temporal, and impact criteria have been developed to discern the proportion of trajectories that interact with the sloping potential surrounding the CI during a reaction. The distance from the incoming H atom to the CI R_{CI} was monitored during each trajectory, along with the product bond length R_{AB}. The first minimum in each of these coordinates, R_{CI}^{min} and R_{AB}^{min} was recorded along with their relative occurrence times.

Trajectories which undergo hard collinear impacts were identified when R_{CI}^{min} was greater than the D_2 internuclear separation q at that point; this is shown in panel (a) of Fig. 12. This means that the incoming atom interacts with the steep repulsive wall of the leading atom of the D_2 molecule and, therefore, does not come close enough to the CI to be influenced by the sloping potential surrounding it. 28% of all reactive trajectories, i.e., leading to all product states, at $E_{col}=1.85$ eV undergo such hard end-on collisions, which are indicative of the direct recoil mechanism. Trajectories with $R_{CI}^{min}>0.858\,474$ Å, the outer turning point of the reactant vibration, do not pass through the circle in panel (b) of

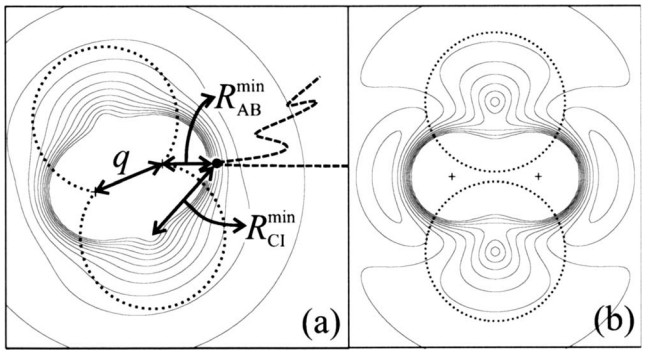

FIG. 12. (a) Impact diagram (cf. Fig. 7) demonstrating the criterion for the assignment of the hard impact mechanism. The dashed circles have a radius of the D_2 internuclear separation q around the conical intersection. (b) For the H_3 PES with a larger D_2 separation, the dashed circles have the radius of the outer turning point of the reactant vibration, 0.858 474 Å. Trajectories that do not pass through the circle have no interaction with the sloping potential around the CI.

Fig. 12 and, thus, can be considered to have no interaction with the sloping potential around the CI. In both cases, the H atom does not pass close enough to the sloping potential around the CI to have any interaction with it.

Trajectories which did not conform to the previous conditions were then assessed with further criteria, based on the relative times of both minima and the proximity of approach of the H atom to the CI and abstracted D atom. For example, a trajectory where R_{CI}^{min} happens before R_{AB}^{min}, and $R_{CI}^{min} < R_{AB}^{min}$ [cf. Fig. 12(a)], is said to hit the sloping potential around the CI. 28% of trajectories were accounted for by this condition and probably undergo a revolving door or LID mechanism. Whereas a trajectory where R_{AB}^{min} happens before R_{CI}^{min} and $R_{CI}^{min} > R_{AB}^{min}$ does not interact with the sloping potential around the CI. These trajectories, along with those that meet the criteria illustrated in Fig. 12(b), account for the 16% of trajectories that do not interact with the CI during the reaction and are currently unassignable. The remaining 28% of trajectories were found to interact with the CI during the reaction in a less well-defined way; some of these trajectories may be involved in an insertion type mechanism.[17,27]

This demonstrates the importance of the potential around the CI at this collision energy (affecting up to 56% of reactive trajectories). We have analyzed trajectories over a wide range of collision energies in search for these new mechanisms and have identified the presence of the LID mechanism, in particular, down to $E_{col}=1.0$ eV, the signatures of which have already been reported in a previous study.[18] These are initial results from an ongoing study of the hydrogen exchange reaction mechanisms.

V. CONCLUSIONS

Results from a QCT study into the hydrogen exchange reaction for the H+D_2 isotopic variant at $E_{col}=1.85$ eV have been presented. The results were used to elucidate new reaction mechanisms which lead to HD($v'=0, j'=0-1$) product states.

The mechanisms responsible for scattering into the HD($v'=0, j'=0$) product state are not of the hard impact or glancing type assumed to be prevalent in this reaction.[1,22] There are at least two new reaction mechanisms present in the collisions leading to $v'=0$ products with little rotational excitation, which do not involve any direct recoil.

The LID mechanism, in which the hydrogen "deflects off" the sloped potential around the CI to form products with the foremost deuterium atom, is dominant, accounting for 74% of reactive trajectories leading to these low j' product states. The revolving door mechanism, in which the CI is used as a lever to cause rotation of the D_2 before scattering to a wide range of angles, corresponds to 21% of these reactive trajectories. The dominance of the LID and revolving door mechanisms demonstrates the importance of the topology of the PES caused by the CI in the reaction dynamics of the hydrogen exchange reaction at high collision energies.

Both the LID and revolving door mechanisms use the sloping potential around the CI to dissipate excess energy and match the speeds of the product atoms so that the first impact of the reactant H atom upon the D atom is at the inner turning point of the $v'=0$ product vibration. This is in contrast to the end-on collisions required by the recoil model, where direct impacts upon the hard wall (steep potential) at the head or tail of the D_2 molecule give the inner turning point of vibrationally highly excited products.

The QCT results were compared to recent time dependent QM calculations.[34] The agreement between the QCT and QM snapshots demonstrates the ability of QCT calculations to physically interpret quantum results by gaining greater insight into the atomic motions during molecular collisions. In particular, this method has the ability to graphically demonstrate the origins of interference phenomena found in QM results.[17,27]

To assess the significance of the new mechanisms to the total reactive scattering, a series of geometric, temporal, and impact criteria have been developed to discern the proportion of trajectories that interact with the sloping potential surrounding the CI during a reaction. Initial studies of the 5×10^6 trajectories calculated at a collision energy of 1.85 eV have shown that 28% of all reactive trajectories undergo hard end-on collisions leading to the direct recoil mechanism. 16% do not interact with the CI during the reaction and are currently unassignable. 28% hit the sloping potential around the CI (and probably undergo a revolving door or LID mechanism). 28% interact with the CI during the reaction in a less well-defined way and may be involved in an insertion type mechanism. The importance of the potential around the CI at this collision energy, affecting up to 56% of reactive trajectories, has been demonstrated.

ACKNOWLEDGMENTS

S.J.G. acknowledges the funding of a studentship by EPSRC and the Department of Chemistry, University of Durham. We thank the EPSRC for financial support. E.W. thanks F. J. Aoiz and L. Bañares for their long-standing collaboration on the hydrogen exchange reaction and for making their QCT code available, parts of which form the basis for the code used in this study. S.C.A. acknowledges the award of a Royal Society University Research Fellowship.

[1] D. G. Truhlar and R. E. Wyatt, Annu. Rev. Phys. Chem. **27**, 1 (1976).
[2] D. G. Truhlar and R. E. Wyatt, Adv. Chem. Phys. **36**, 141 (1977).
[3] G. C. Schatz, Annu. Rev. Phys. Chem. **39**, 317 (1988).
[4] H. Buchenau, J. P. Toennies, J. Arnold, and J. Wolfrum, Ber. Bunsenges. Phys. Chem. **94**, 1231 (1990).
[5] W. H. Miller, Annu. Rev. Phys. Chem. **41**, 245 (1990).
[6] F. Fernández-Alonso and R. N. Zare, Annu. Rev. Phys. Chem. **53**, 67 (2002).
[7] F. J. Aoiz, L. Bañares, and V. J. Herrero, Int. Rev. Phys. Chem. **24**, 119 (2005).
[8] L. Bañares, F. J. Aoiz, and V. J. Herrero, Phys. Scr. **73**, C6 (2006).
[9] N. C. Blais, M. S. Zhao, and D. G. Truhlar, Chem. Phys. Lett. **166**, 11 (1990).
[10] W. H. Miller and J. Z. H. Zhang, J. Phys. Chem. **95**, 12 (1991).
[11] B. K. Kendrick, J. Phys. Chem. A **107**, 6739 (2003).
[12] S. C. Althorpe, J. Chem. Phys. **114**, 1601 (2001).
[13] M. Hankel, S. C. Smith, R. J. Allan, S. K. Gray, and G. G. Balint-Kurti, J. Chem. Phys. **125**, 164303 (2006).
[14] E. Wrede, L. Schnieder, K. H. Welge, F. J. Aoiz, L. Bañares, V. J. Herrero, and B. Martínez-Haya, J. Chem. Phys. **110**, 9971 (1999).
[15] F. Fernández-Alonso, B. D. Bean, J. D. Ayers, A. E. Pomerantz, R. N. Zare, L. Bañares, and F. J. Aoiz, Angew. Chem., Int. Ed. **39**, 2748 (2000).
[16] F. J. Aoiz, L. Bañares, M. J. D'Mello, V. J. Herrero, V. Sáez Rábanos, L. Schnieder, and R. E. Wyatt, J. Chem. Phys. **101**, 5781 (1994).
[17] J. C. Juanes-Marcos, S. C. Althorpe, and E. Wrede, J. Chem. Phys. **126**, 044317 (2007).
[18] F. J. Aoiz, V. J. Herrero, and V. S. Rábanos, J. Chem. Phys. **97**, 7423 (1992).
[19] F. J. Aoiz, V. J. Herrero, and V. S. Rábanos, J. Chem. Phys. **95**, 7767 (1991).
[20] F. J. Aoiz, V. J. Herrero, and V. S. Rábanos, J. Chem. Phys. **94**, 7991 (1991).
[21] F. J. Aoiz, L. Bañares, and V. J. Herrero, J. Chem. Soc., Faraday Trans. **94**, 2483 (1998).
[22] D. E. Manolopoulos, Nature (London) **419**, 266 (2002).
[23] S. C. Althorpe, F. Fernández-Alonso, B. D. Bean, J. D. Ayers, A. E. Pomerantz, R. N. Zare, and E. Wrede, Nature (London) **416**, 67 (2002).
[24] S. C. Althorpe, J. Chem. Phys. **117**, 4623 (2002).
[25] S. A. Harich, D. X. Dai, C. C. Wang, X. M. Yang, S. D. Chao, and R. T. Skodje, Nature (London) **419**, 281 (2002).
[26] S. J. Greaves, D. Murdock, and E. Wrede, J. Chem. Phys. **128**, 164307 (2008).
[27] J. C. Juanes-Marcos, S. C. Althorpe, and E. Wrede, Science **309**, 1227 (2005).
[28] D. G. Truhlar and J. T. Muckerman, *Atom-Molecule Collision Therory: A Guide for the Experimentalists*, edited by R. B. Bernstein (Plenum, New York, 1979), pp. 505–566.
[29] A. Ralston and H. Wilf, *Mathematical Methods for Digital Computers* (Wiley, London, 1960).
[30] L. Bañares, F. J. Aoiz, P. Honvault, B. Bussery-Honvault, and J.-M. Launay, J. Chem. Phys. **118**, 565 (2003).
[31] A. J. Dobbyn, P. McCabe, J. N. L. Connor, and J. F. Castillo, Phys. Chem. Chem. Phys. **1**, 18 1115 (1999).
[32] A. I. Boothroyd, W. J. Keogh, P. G. Martin, and M. R. Peterson, J. Chem. Phys. **104**, 7139 (1996).
[33] Animations of trajectories of the mechanisms described in this paper can be accessed at http://www.durham.ac.uk/eckart.wrede/QCT/mechanisms/.
[34] S. C. Althorpe, J. Chem. Phys. **121**, 1175 (2004).
[35] J. N. L. Connor, Phys. Chem. Chem. Phys. **6**, 377 (2004).
[36] D. Sokolovski, Chem. Phys. Lett. **370**, 805 (2003).